NASA Technical Memorandum 81219

Turbulent Structures in Wall-Bounded Shear Flows Observed Via Three-Dimensional Numerical Simulations

A. Leonard

July 1980

National Aeronautics and Space Administration

NASA Technical Memorandum 81219

Turbulent Structures in Wall-Bounded Shear Flows Observed Via Three-Dimensional Numerical Simulations

A. Leonard, Ames Research Center, Moffett Field, California

National Aeronautics and
Space Administration

Ames Research Center
Moffett Field, California 94035

TURBULENT STRUCTURES IN WALL-BONDED SHEAR FLOWS OBSERVED VIA THREE-DIMENSIONAL NUMERICAL SIMULATIONS

A. Leonard
Ames Research Center, NASA
Moffett Field, California 94035, U.S.A.

I. INTRODUCTION

In the past few years, numerical techniques in fluid dynamics have matured to the point that meaningful simulations of three-dimensional transitional or turbulent shear flows bounded by a wall are possible. At the same time, availability of advanced computers, over and above a CDC 7600-class machine, has allowed roughly a doubling of the spatial resolution in each direction, greatly enhancing the quality of the results. We are in a position now to expand our set of objectives for flow simulations in the next decade to the following:

1. Increase our understanding of the physics of turbulence
2. Provide statistical and other information useful to turbulence modelers
3. Provide a testbed for the development of improved numerical methods and guidance for improved modeling of fine-scale effects.

Objectives (1) and (2) are, of course, in common with the goals of most experimental (and purely theoretical) investigations of turbulent flows. The numerical simulation, however, provides a different way to look at a turbulent flow; the results of computer simulations are complementary to those of laboratory experiments. In the computer experiment, the corresponding laboratory time of the simulation is relatively small, but complete flow-field information is available throughout that time interval. The third objective is related to the desire to improve future simulations and to make it possible to investigate more complex flows. Advanced computers, as they become available, will also help in this regard.

In this paper we report on three recent simulations, using the ILLIAC IV computer, that begin to meet the above objectives:

1. Study of the evolution of a wave-like disturbance in a laminar boundary layer corresponding to vibrating-ribbon experiments.
2. Study of the evolution of a spot-like disturbance in a laminar boundary layer.
3. Investigation of turbulent channel flow.

In particular, we will concentrate on the turbulent structures observed in these flow simulations and comment on their role (1) in the dynamical process, for example, the growth and maintenance of turbulence, and (2) as contributors to turbulent statistics of interest to turbulence modelers. As will be shown, these persistent flow structures include streamwise and vertical vorticity distributions near the wall, low-speed and high-speed streaks, and local regions of intense vertical velocity.

The problem of representing the large range of physical scales in a computer simulation will also be discussed, along with some prospects for future improvement.

Quite different numerical techniques are employed in the three simulations. The first and third simulations listed above use an Eulerian grid with pressure and velocity as dependent variables and periodic boundary conditions in two directions, whereas the second simulation uses a Lagrangian vortex method in a semi-infinite domain. The first two simulations studied the evolution in time of an initial disturbance and have no explicit model to account for "subgrid-scale" turbulence — fine-scale structures not resolvable by the computational mesh. Consequently, in these simulations the evolution time during which meaningful results were obtained was limited, due to the importance of subgrid effects at later times. In the study of turbulent channel flow, however, the objective was to simulate a fully developed turbulent flow having a range of scales much larger than the computational mesh would allow. Thus, the use of a subgrid model was mandatory. In Section II, further details of the simulations are given along with major findings regarding the observed turbulent structures. The problem of accounting for turbulence scales not resolved or represented by the computational mesh — subgrid or supergrid modeling or both — is discussed in Section III, and some possibilities for improvement are suggested. In Section IV, a summary of the results and conclusions are presented.

II. RESULTS OF THREE NUMERICAL SIMULATIONS

A. Flat-Plate Transition

In a series of computer experiments Wray and Hussaini [1] (hereinafter referred to as WH) studied the instability of a flat-plate boundary layer in three dimensions by solving numerically the incompressible Navier-Stokes equations. In another three-dimensional numerical study, Orszag and Kells [2] investigated transition of plane Poiseuille and plane Couette flow. The ILLIAC computer code of WH is capable of simulating a wide range of boundary-layer stability problems. In this particular investigation they simulated the vibrating-ribbon experiments of Kovasznay et al. [3] by a careful choice of initial conditions for the three-dimensional perturbation to the Blasius profile. Two oblique (three-dimensional) eigensolutions of the Orr-Sommerfeld equation were added to a two-dimensional eigensolution to form the initial perturbation. To correspond with the laboratory experiment the streamwise and spanwise wavelengths of the perturbation waves were 25.2 δ^* and 30 δ^*, respectively, where δ^* is the initial displacement thickness of the laminar boundary layer. A schematic of the numerical simulation of WH is shown in Fig. 1. Wray and Hussaini used Fourier expansions (spectral method) in the streamwise (x) and spanwise (z) directions with 64 points each and second-order finite differences in the normal (y) direction with 128 points on a stretched mesh. Fourier transformation of the momentum and mass

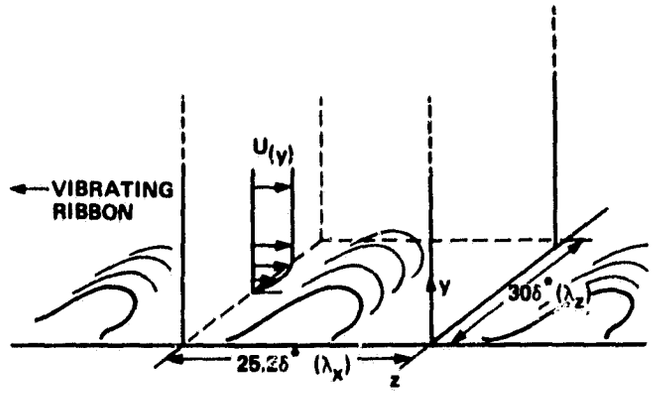

GRID: 64 × 128 × 64
BOUNDARY CONDITIONS:
$\underline{u}(\underline{x}) = 0$ at $y = 0$
$\underline{u}(\underline{x}) \to U_\infty \hat{e}_x$ as $y \to \infty$
PERIODIC IN x AND z

FIG. 1 Simulation of a wave-like disturbance in a laminar boundary layer.

conservation equations in x and z and some manipulations to minimize storage requirements yield the following system of equations for every (k_x, k_z):

$$\frac{\partial \hat{u}}{\partial t} + ik_x(\hat{u^2} - \hat{v^2}) + \frac{\partial \hat{uv}}{\partial y} + ik_z\hat{uw} + ik_x\hat{q} = -\nu k^2\hat{u} + \nu\frac{\partial^2\hat{u}}{\partial y^2} ; \tag{1}$$

$$\frac{\partial \hat{v}}{\partial t} + ik_x\hat{uv} + ik_z\hat{vw} + \frac{\partial \hat{q}}{\partial y} = -\nu k^2\hat{v} + \nu\frac{\partial^2\hat{v}}{\partial y^2} ; \tag{2}$$

$$\frac{\partial \hat{w}}{\partial t} + ik_x\hat{uw} + \frac{\partial \hat{vw}}{\partial y} + ik_z(\hat{w^2} - \hat{v^2}) + ik_z\hat{q} = -\nu k^2\hat{w} + \nu\frac{\partial^2\hat{w}}{\partial y^2} ; \tag{3}$$

$$ik_x\hat{u} + \frac{\partial \hat{v}}{\partial y} + ik_z\hat{w} = 0 . \tag{4}$$

Equations (1)-(4) give the time evolution of the Fourier transformed velocity components $\hat{u}$, $\hat{v}$, $\hat{w}$ and a pseudopressure $\hat{q} = \hat{p} + \hat{v^2}$. Here $k^2 = k_x^2 + k_z^2$. In computing the nonlinear terms above, WH zero any aliasing contributions by the 2/3 rule, yielding a calculation that is equivalent to a Galerkin spectral method with 22 wave numbers in the x and z directions.

The use of periodic boundary conditions in the streamwise direction leads to an evolution of the disturbance in time rather than space and to a slight departure from the Blasius profile. However, this assumption allows WH to apply 64 grid points (22 wave numbers) to each wavelength of the disturbance, thereby achieving high resolution of streamwise variations in the flow field. In the laboratory experiment, the evolution of the disturbance occurs in space over a distance of about 10 wavelengths. Thus, in the laboratory a particular structure at one streamwise location is a neighbor to the same structure located 1 wavelength downstream, but in a slightly

advanced state of evolution. Similarly, an earlier state of that structure is situated 1 wavelength upstream. As found by WH, however, the difference between the spatial and temporal developments in the linear part of the evolution (exponential growth) is quite small as measured by the amplitudes and phases of the eigenmodes of the two problems. Apparently the nonlinear evolution is very similar as well, judging by the excellent agreement between the two experiments. In Fig. 2 are shown contours of $\partial u/\partial y$ for both the laboratory experiment and the computer simulation at the one-spike stage — the spike being the kink in the high amplitude $\partial u/\partial y$ contours [3]. The contours are taken in the x-y plane containing the maximum initial perturbation — the peak plane. At this point the time of evolution in the simulation is 340 δ^*/U_∞. The agreement is quite good as is the comparison of the corresponding normal velocity contours given in Fig. 3. The maximum vertical velocity is roughly 0.07 U_∞ at this stage. The boundary-layer thickness, δ, is approximately 3 times the displacement thickness.

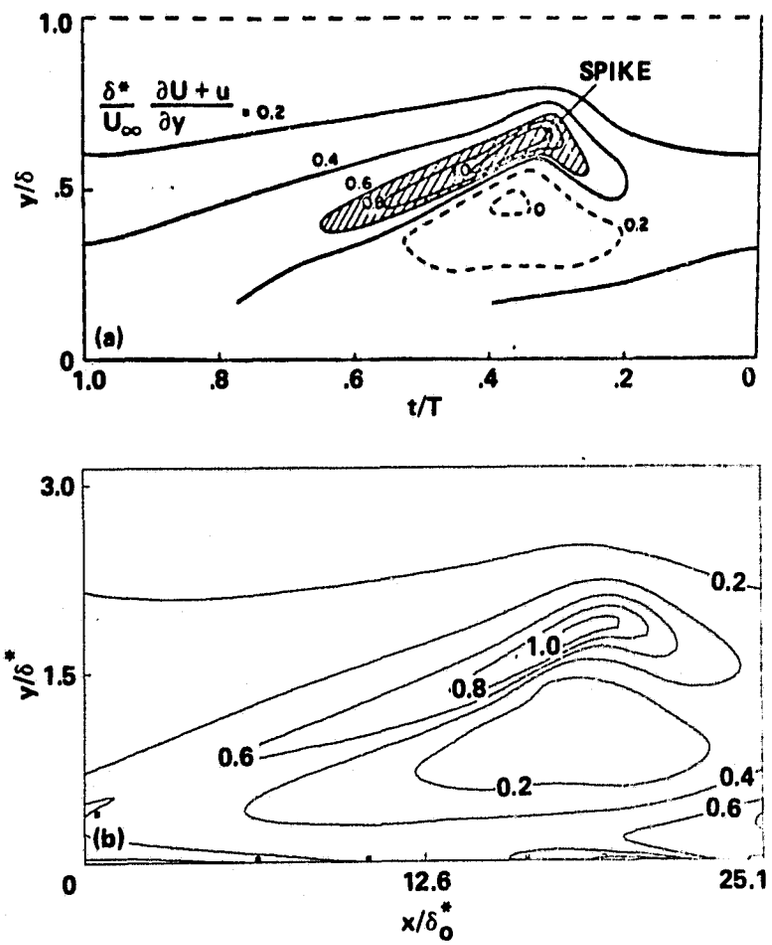

FIG. 2 Contours of $\partial u/\partial y$ in peak plane — one-spike stage: (a) experiment [3]; (b) numerical simulation of WH.

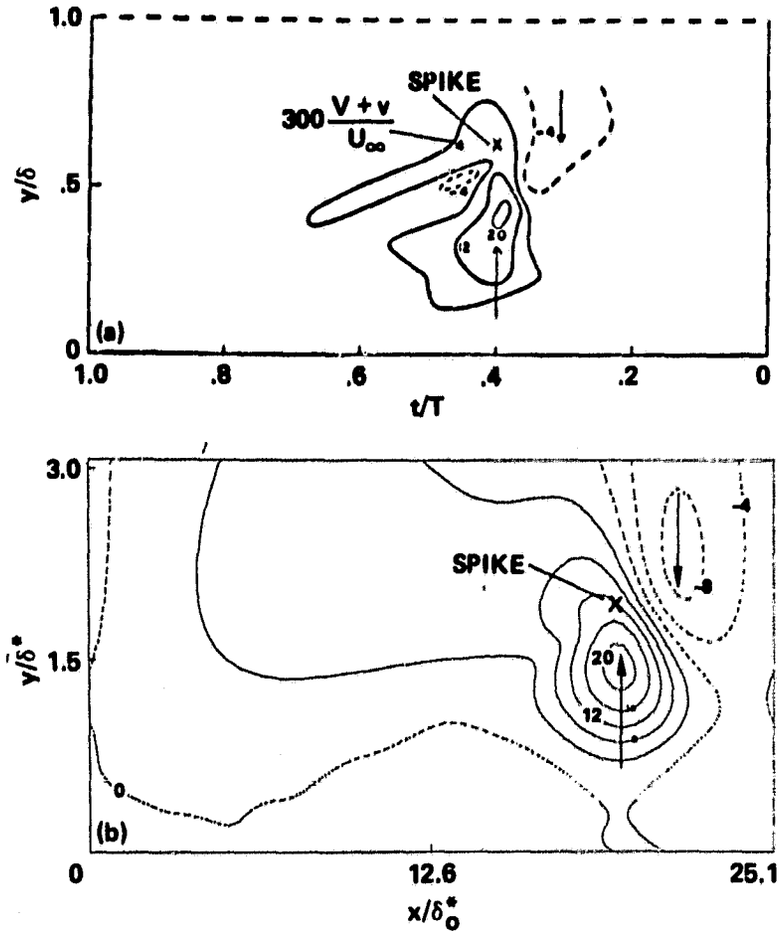

FIG. 3 Vertical velocity in peak plane — one-spike stage: (a) experiment [3]; (b) numerical simulation of WH.

As nonlinear effects become increasingly significant, the evolution of the computational disturbance reaches the two-spike stage at $t = 360\ \delta^*/U_\infty$. Contours of $\partial u/\partial y$ and normal velocity at this stage are shown in Figs. 4 and 5, respectively. Note that again there is very good agreement on the structure of the disturbance in the peak plane. The relative shift of the structures along the abscissa is irrelevant [1], but other discrepancies are evident. For example, the computation is producing peak values in v ($\approx 0.21\ U_\infty$) that are higher than the experiment. Considering the large streamwise gradient of v in the vicinity of this maximum, it is quite possible that this type of discrepancy is due to lack of resolution or to ensemble averaging or both in the laboratory experiment. On the other hand, the appearance of oscillatory fine-scale features in Fig. 4 indicates that the computation may be starting to have a resolution problem also. A three-spike stage occurs in the simulation at $t \approx 365\ \delta^*/U_\infty$. Soon after this time significant errors begin to appear due to the fact that the energy of the disturbance is trapped to remain within the computational wave numbers.

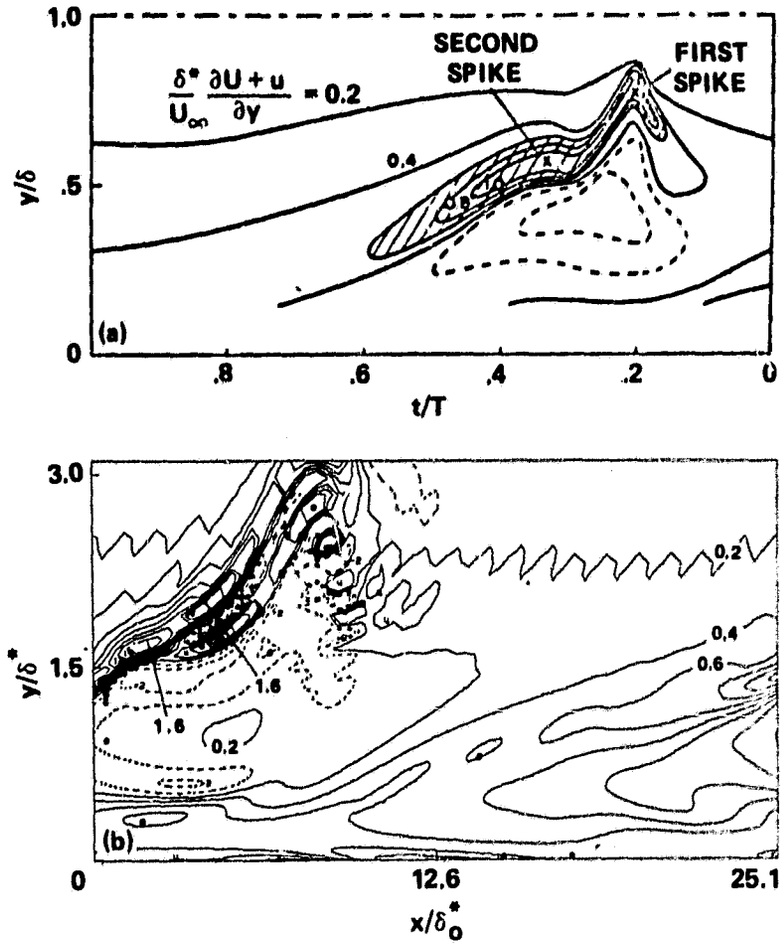

FIG. 4 Contours of $\partial u/\partial y$ in peak plane — two-spike stage: (a) experiment [3]; (b) numerical simulation of WH.

Thus, in a remarkable computational effort WH have demonstrated the capability of simulating a complex, three-dimensional transitional flow in an "honest" calculation — no subgrid modeling was used. In the particular case that was stimulated the results appear to be valid up to and including the two-spike stage when $v_{max} \approx 0.21\ U_\infty$. After that stage, presumably, scales with wavelengths $\leq 30\delta^*/22$ in the spanwise direction or $\leq 25\delta^*/22$ in the streamwise direction become important. The vertical resolution appears to be quite adequate throughout the simulation.

B. Spot-Like Disturbance in a Laminar Boundary Layer

In another numerical investigation of boundary-layer mechanics, Leonard [4] studied the growth of localized disturbances in a laminar boundary layer as they evolve into spot-like turbulent structures. As in the study of WH, these are computer experiments, but using a quite different numerical method. Vortex filaments are used to represent the three-dimensional, perturbed vorticity field within the spot. Each filament is defined by a three-dimensional space curve $\underline{x}(\xi,t)$, circulation Γ, and a

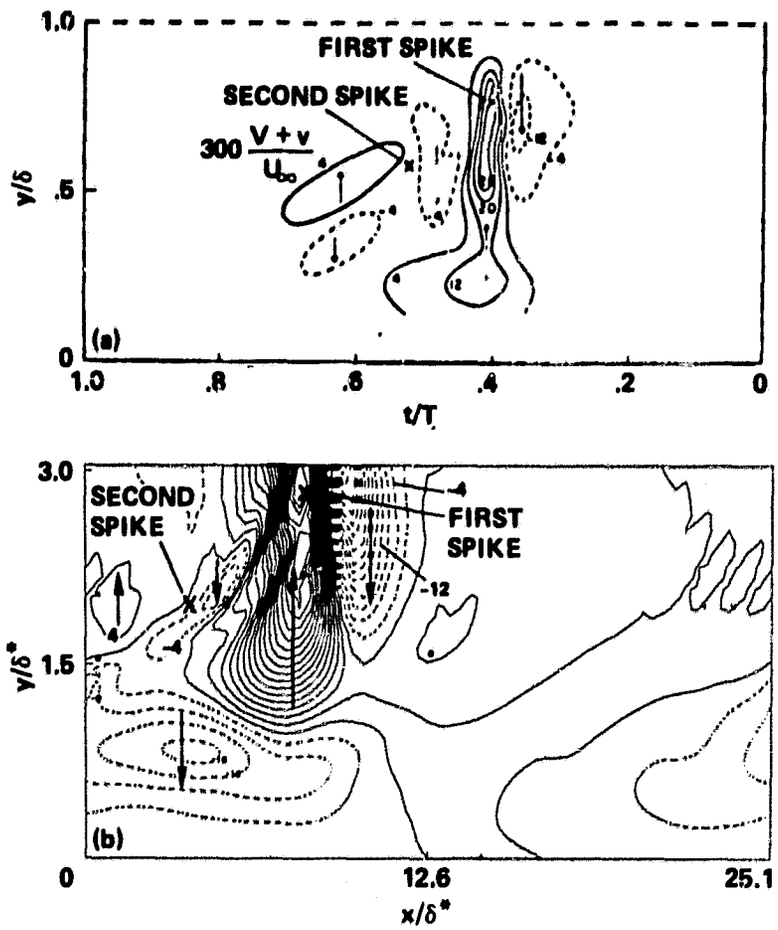

FIG. 5 Vertical velocity in peak plane — two-spike stage: (a) experiment [3]; (b) numerical simulation of WH.

core size, σ, which parameterizes an assumed Gaussian vorticity within the core. Thus, the perturbed vorticity field is given by a summation over filaments,

$$\underline{\omega}'(\underline{x},t) = \sum_i \Gamma_i \int_{c_i} \exp[-|\underline{x} - \underline{x}_i|^2/\sigma^2] \Big/ (\sqrt{\pi}\sigma)^3 (\partial \underline{x}_i/\partial \xi) d\xi \ . \tag{5}$$

The vortex filaments represent a continuum of vorticity which initially is in the form of an infinite sheet of finite thickness, that is, a boundary layer. As indicated in the schematic (Fig. 6) the disturbance in the simulation is created by a local distortion of the vortex filaments at $t = 0$. For numerical purposes each tube of vorticity in the boundary layer is decomposed into its straight, unperturbed contribution and into a loop representing its contribution to the perturbed vorticity field, as shown in Fig. 7. The velocity field is decomposed, accordingly, as

$$\underline{u}(\underline{x}) = U(y)\hat{e}_x + \underline{u}'(\underline{x}) \ , \tag{6}$$

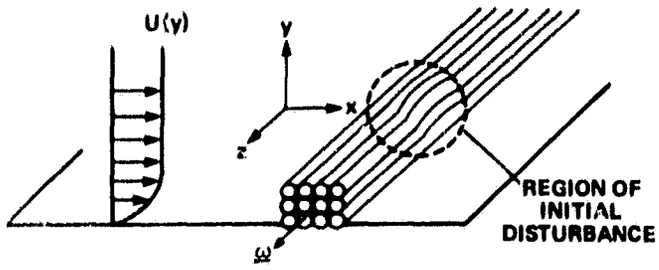

GRID: 500 VORTEX FILAMENTS, 8000 NODE POINTS } AT $t = t_{max}$

BOUNDARY CONDITIONS:

FLOW TANGENCY AT $y = 0$

$\underline{u}(\underline{x}) \to U(y)\,\hat{e}_x \quad |\underline{x}| \to \infty$

FIG. 6 Simulation of a spot-like disturbance in a laminar boundary layer.

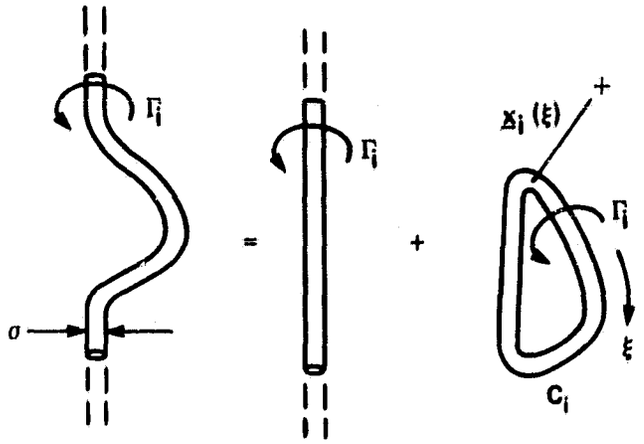

FIG. 7 Decomposition of vorticity field.

where $U(y)$ is the laminar profile and $\underline{u}'$ is given by a sum of Biot-Savart integrations over all the filament curves, C_j, plus their images. The curves are marked with a sequence of node points that are tracked in a Lagrangian reference frame, according to the following equation of motion:

$$\frac{\partial \underline{x}_i}{\partial t} = -\frac{1}{4\pi}\sum_j \Gamma_j \int_{C_j} \times \frac{(\underline{x}_i - \underline{x}_j)\times(\partial \underline{x}_j/\partial \xi')\,d\xi'}{\left[|\underline{x}_i - \underline{x}_j|^2 + \alpha(\sigma_i^2 + \sigma_j^2)\right]^{3/2}}$$

$$+ \hat{e}_x\, U(y) + \text{image contributions.} \qquad (7)$$

The equation is seen to be the Biot-Savart induction law for an infinitesimal filament, but corrected in the near-field for finite core size. Using $\alpha = 0.2065$ we recover the correct speed of a ring vortex in the limit $\sigma \ll$ ring radius. Up to numerical truncation error, the method simulates the inviscid dynamics of the vorticity field and therefore satisfies the Kelvin and Helmholtz theorems. For a more complete description of the method including simulation of viscous effects see [5].

Biot-Savart integration yields exact boundary conditions at infinity in all directions. The image contributions ensure tangency of the flow at the wall. In this initial study we ignore the generation of vorticity at the wall boundary due to the disturbance, that is, we use the inviscid boundary condition at the wall for $\underline{u}'$. This appears justified because the relatively high initial disturbance level ($0.07 - 0.10\ U_\infty$) and the initially small length scale of the perturbation $\sim O(\delta^*)$ (corresponding to laboratory experiments on turbulent spots [6,7]) leads to the rapid evolution of a sizable, strong disturbance at the end of the simulation, $t \approx 50\delta^*/U_\infty$. The viscous length scale for this time, assuming $Re_{\delta^*} = 1000$, is only $0.3\delta^*$.

Computational filaments are added automatically as the disturbance grows in size. At the end of the simulation, about 8000 points represent one half of the spot

(symmetry of the flow about the midplane is enforced). The computation could continue beyond this time, but (1) some of the filaments are quite stretched at this point, indicating that remeshing is required, and (2) the cpu time per time step is quite large at this stage being proportional to the square of the number of computational points for vortex methods. Total run times are ≈2 hr on the ILLIAC.

In Fig. 8, the space curves defining the vortex filaments originally in a single layer (out of a total of six representing the boundary layer) are shown at three different times. The spreading of the disturbance and the increasing deformations suffered by the vortex lines are quite evident. In Fig. 9, vertical and streamwise vorticity contour plots at a late time are shown in horizontal (x-z) and spanwise-vertical (z-y) planes, respectively. Note the development of intense streamwise and vertical vorticity generated in the flow in agreement with the pattern of vortex lines displayed in Fig. 8. The structures are cell-like, $O(\delta^*)$ in the spanwise and vertical directions, but elongated in the streamwise direction. For example, the region of negative ω_y just above the x-axis in Fig. 9a together with its antisymmetric counterpart (not shown) just below the axis would constitute one cell approximately $4\delta^*$ in spanwise extent. Velocity contour plots are shown in the same (x-z) and (y-z) planes in Figs. 10 and 11, respectively. The presence of streaky structures in the horizontal plane is compatible with experimental observations of passive particle motion in turbulent spots [7] and turbulent boundary layers [8]. The maximum normal velocity is quite high at $\approx 0.4\ U_\infty$.

Most laboratory experiments on turbulent spots report ensemble-averaged measurements several hundred δ^* downstream of the initial disturbance. A typical streamwise velocity history plot from Cantwell et al. [7] measured in the midplane of the spot is shown in Fig. 12a. Note that compared with the laminar profile there is a velocity excess near the wall and a defect away from the wall — typical of a turbulent boundary-layer profile. The experiment of Wygnanski et al. [6] produced similar results. However, as indicated in Figs. 10 and 11, the particular numerical simulation presented above yields a velocity excess in the midplane for all heights above the boundary. On the other hand, if the velocity field from the numerical simulation is span-averaged over one cell of width $4\delta^*$ centered on the midplane we obtain the velocity plots shown in Fig. 12b. (To obtain better statistics, the results shown in Fig. 12b are based on the velocity field at a single time late in the simulation. Thus, decreasing x is used along the simulation rather than increasing time.) Note the close similarity in the behavior of these computational results averaged over one cell in the span direction at $t = 43\ \delta^*/U_\infty$ to the ensemble-averaged laboratory measurements of Fig. 12a, taken at a fixed streamwise location, at later times ($t \gtrsim 1500\ \delta^*/U_\infty$). The good comparison leads to the speculation that the internal structure of a single realization of a large turbulent spot ($\gtrsim 100\delta^*$ in streamwise extent) is dominated by the presence of many cell-like substructures such as those revealed in the numerical simulation. (For experimental support of this speculation see I. Wygnanski, these proceedings.)

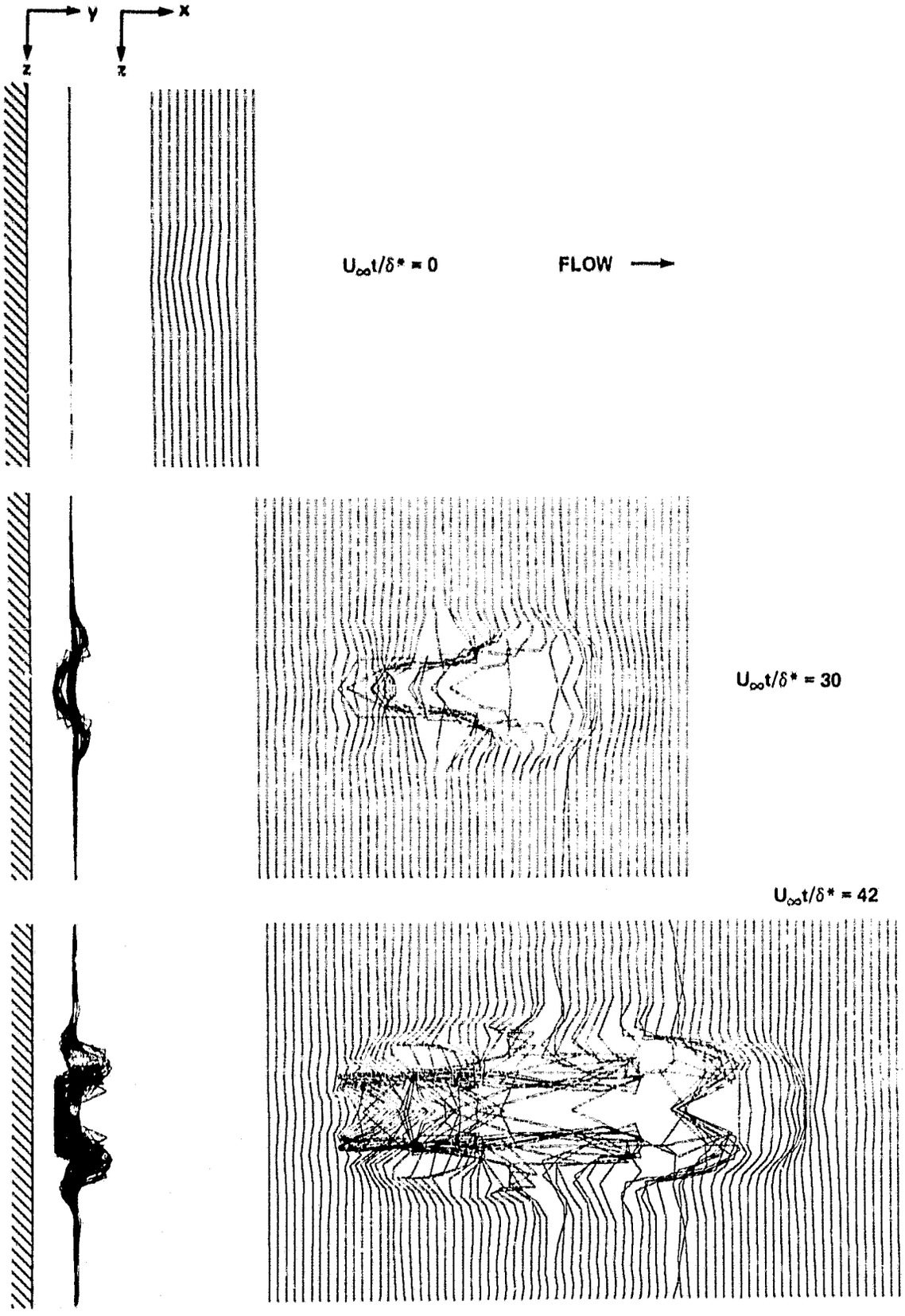

FIG. 8 Top and rear views of one plane of the computed vortex lines.

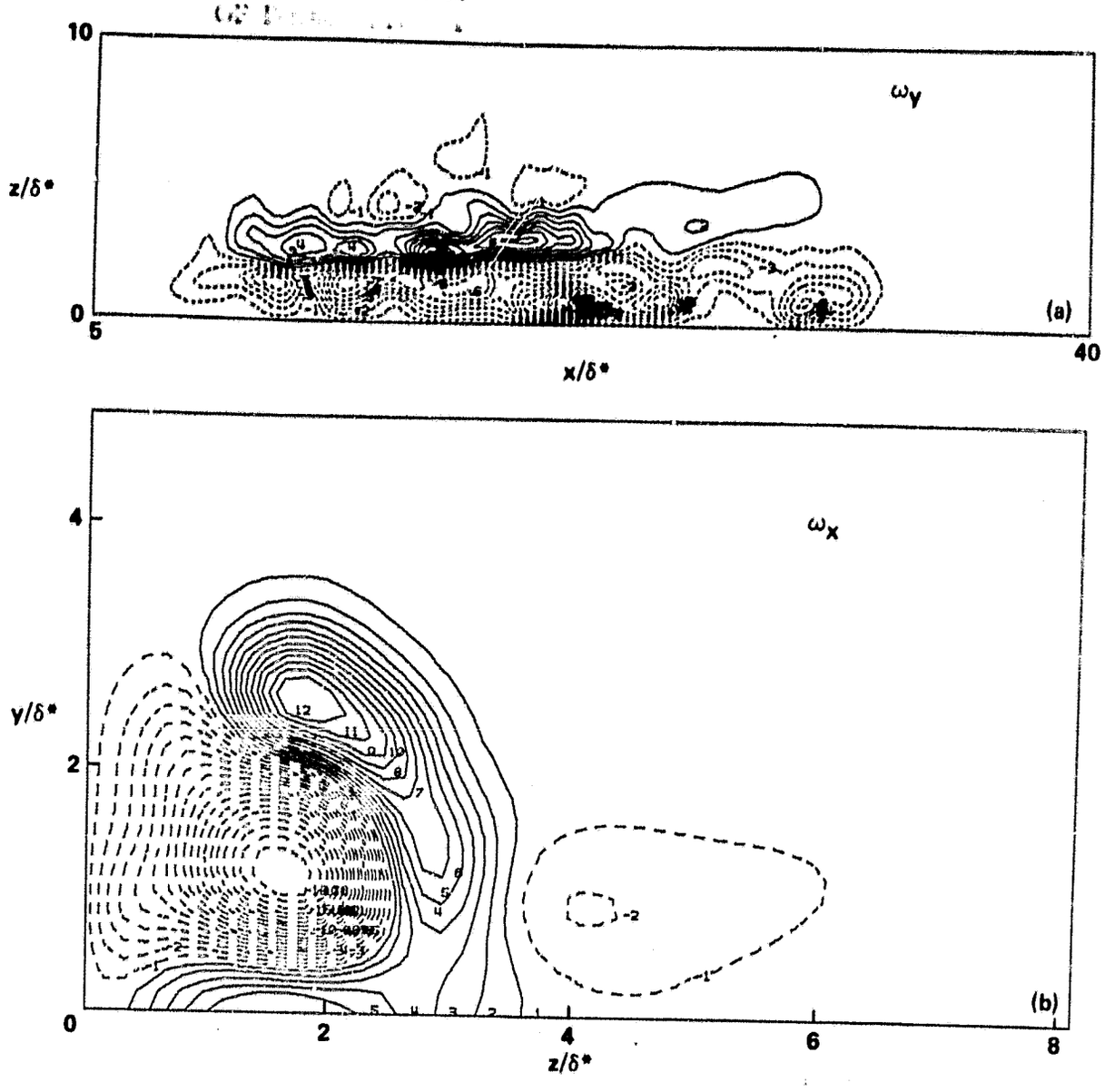

FIG. 9 Contours of vorticity for $U_\infty t/\delta^* = 41$: (a) ω_y in a horizontal plane, $y/\delta^* = 0.66$; (b) ω_x in a vertical (z-y) plane $x/\delta^* = 25$. ——, positive contours; — — —, negative contours; contour levels ±0.05, ±0.15, ±0.25 . . . of $\partial u/\partial y|_{wall}$.

Three-dimensional vortex simulations have therefore demonstrated the rather rapid, nonlinear evolution of small localized disturbances in a laminar boundary layer. The boundary layer appears to deform into a corrugated surface with significant amounts of streamwise and vertical vorticity — leading to strong negative u'v correlations and, hence, intense turbulent mixing. Velocity perturbations induced in the nearby, relatively undisturbed vorticity layer lead to sufficient deformations in the vortex lines to produce local nonlinear growth. Thus, the spot appears to grow in the spanwise direction by "transverse contamination," in agreement with recent experiments using dye interjection [9], which demonstrated that turbulent convection is not

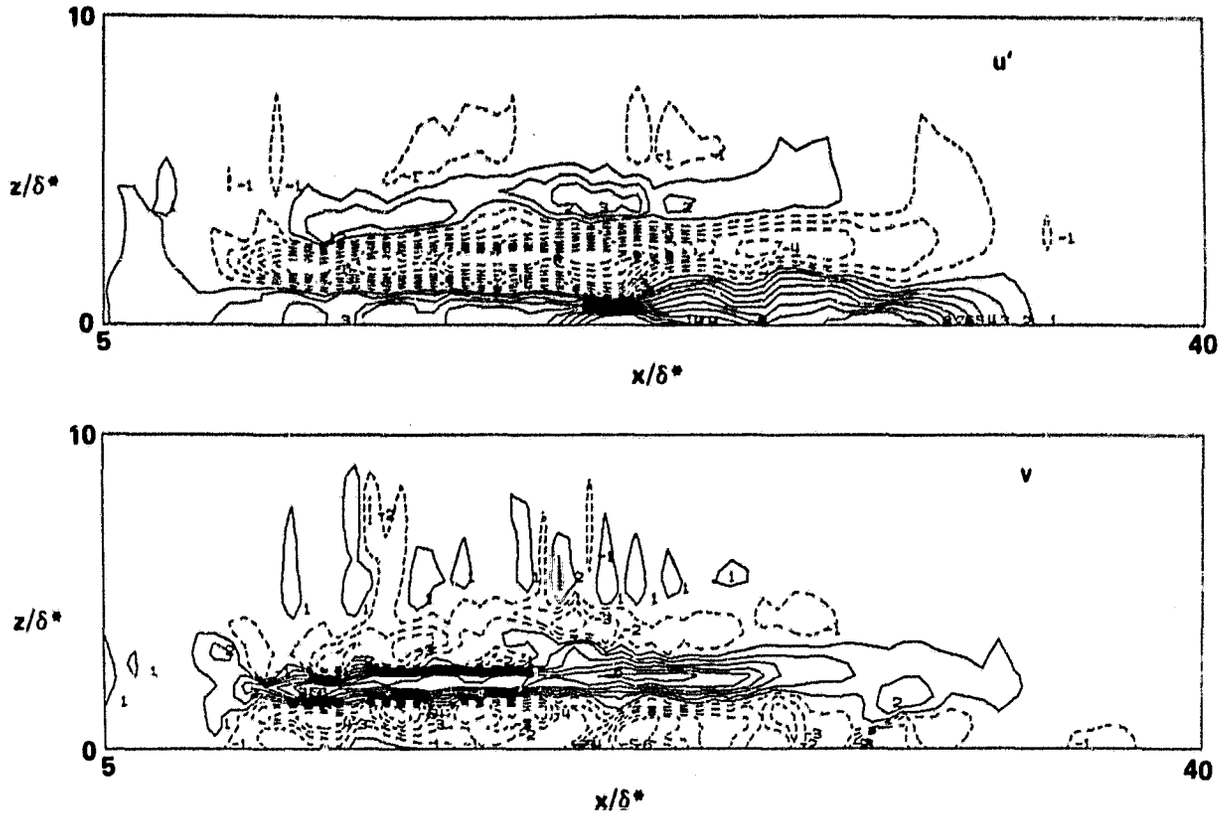

FIG. 10 Velocity contours in the horizontal plane of Fig. 9a. Contour levels ±0.02, ±0.06, ±0.10 . . . of U_∞.

responsible for the spanwise growth of a spot. Further study is needed to simulate properly larger turbulent spots or a collection of spots and the decay of turbulence rearward of the spot.

C. Turbulent Channel Flow

In our third example of a wall-bounded shear flow we discuss the numerical simulation of turbulent channel flow by Kim and Moin [10] (hereinafter referred to as KM). As shown in Fig. 13, a 64^3 grid is used to simulate flow at Re = 13,800 with periodic boundary conditions in the spanwise and streamwise directions and the no-slip condition at the channel walls. In an earlier investigation of turbulent channel flow, Moin et al. [11] used a 16×64×16 grid with the same boundary conditions. Because the laboratory flow at this Reynolds number contains a significant amount of turbulent energy at length scales smaller than the computational grid, KM used the filtered Navier-Stokes equations to determine the dynamics of the turbulence field that is resolvable on their mesh (large eddy simulation technique). Thus, a flow variable f may be decomposed as follows:

$$f = \bar{f} + f' \ , \qquad (8)$$

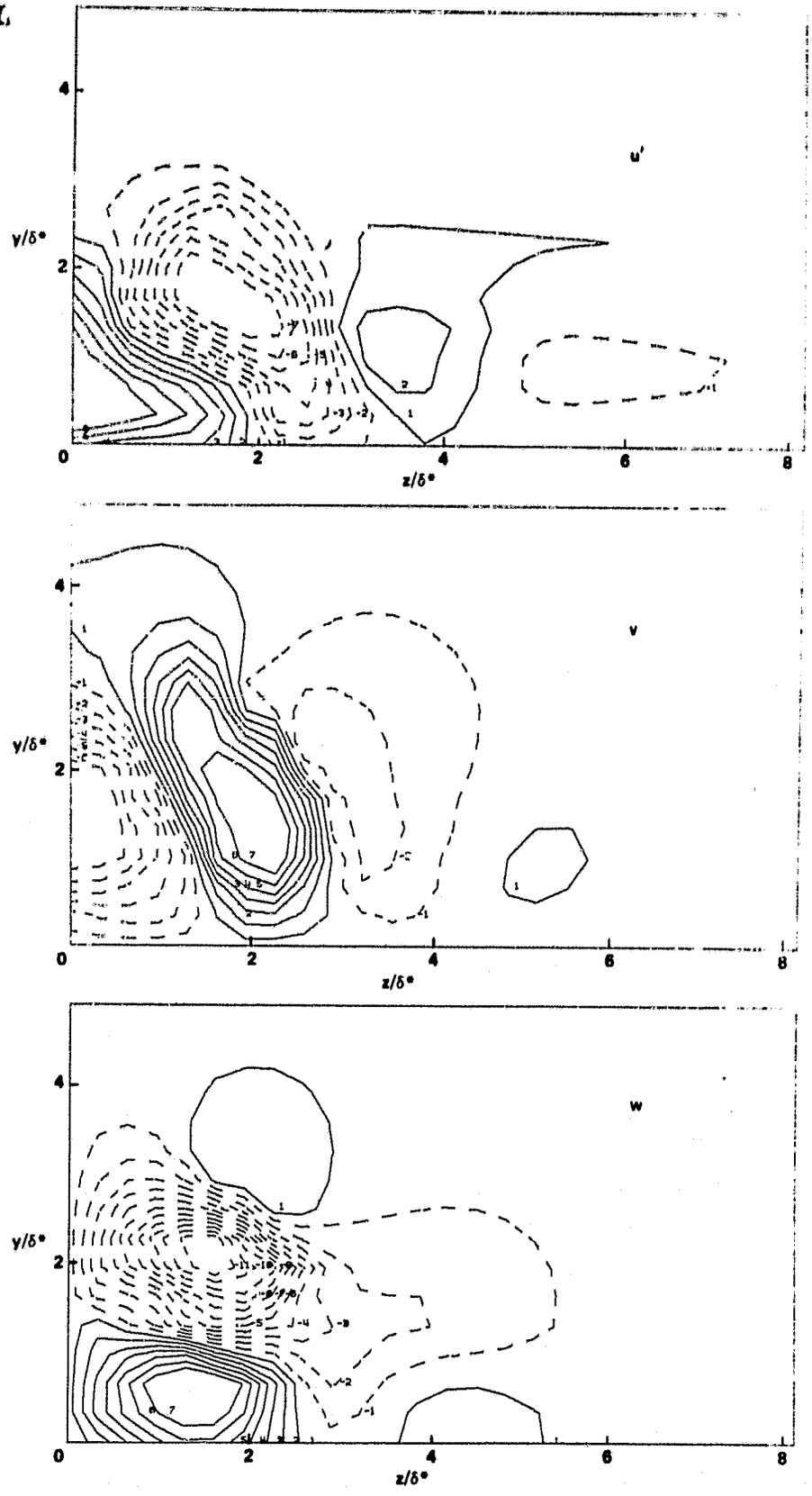

FIG. 11 Velocity contours in the vertical plane of Fig. 9b.
Same contour levels as Fig. 10.

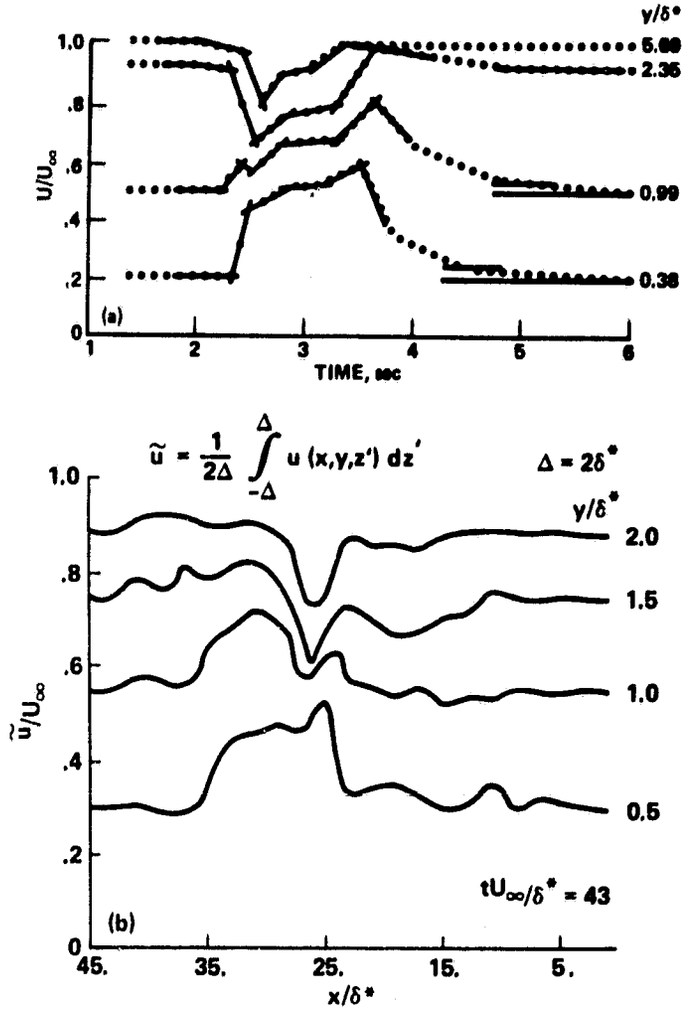

FIG. 12 Streamwise velocity: (a) ensemble-average velocity records [7], $x/\delta_0^* \approx 1600$; (b) cell-averaged streamwise velocity from numerical simulation of [4].

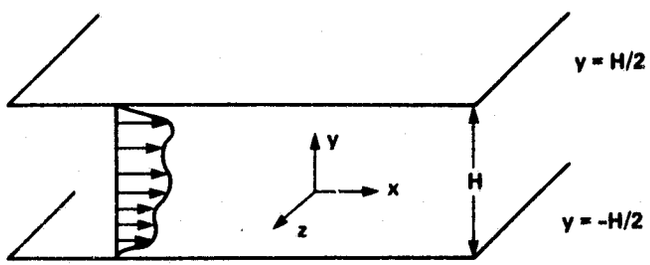

$Re = \frac{U_c H/2}{\nu} = 13800$
GRID: 64 × 64 × 64
BOUNDARY CONDITIONS:
u = v = w = 0, AT y = ± H/2
PERIODIC IN x AND z

FIG. 13 Numerical simulation of turbulent channel flow.

where $\bar{f}$ is the large-scale field, defined as the result of a filtering or smoothing operation of f, and f' is the subgrid field.

After applying the filtering operation to the incompressible momentum and continuity equations, the governing equations for the filtered field may be written

$$\frac{\partial \bar{\underline{u}}}{\partial t} + \overline{\underline{\omega} \times \underline{u}} = -\nabla p^* + \frac{dP}{dx}\hat{e}_x - \nabla \cdot \underline{\tau} + \nu \nabla^2 \bar{\underline{u}} \qquad (9)$$

and

$$\nabla \cdot \bar{\underline{u}} = 0 , \qquad (10)$$

where dP/dx is the constant mean pressure gradient, $\bar{\underline{\omega}}$ is the large-scale vorticity field, and the subgrid-scale stress tensor, $\underline{\tau}$, (having zero trace) has components defined by

$$\tau_{ij} = R_{ij} - R_{kk}/3\ \delta_{ij} \qquad (11)$$

and

$$R_{ij} = \overline{u_i' u_j'} + \overline{u_j' \bar{u}_i} + \overline{\bar{u}_j u_i'} . \qquad (12)$$

The quantity p^* is given by

$$p^* = \bar{p}/\rho + 1/2\ \overline{\bar{u}_k \bar{u}_k} + R_{kk}/3 . \qquad (13)$$

The system of equations (9) and (10) becomes deterministic once $\underline{\tau}$ is specified. Kim and Moin use an eddy viscosity model,

$$\tau_{ij} = -2\nu_T S_{ij} , \qquad (14)$$

where

$$S_{ij} = \frac{1}{2}\left(\frac{\partial \bar{u}_i}{\partial x_j} + \frac{\partial \bar{u}_j}{\partial x_i}\right) , \qquad (15)$$

and ν_T is given by the Smagorinsky model,

$$\nu_T = (C_S \Delta)^2 \sqrt{S_{ij} S_{ij}} . \qquad (16)$$

The constant C_S is taken to be 0.1 and Δ is a measure of the grid resolution and is taken to be

$$\Delta = (\Delta x\, \Delta y\, \Delta z)^{1/3}[1 - \exp(-y^+/50)] \tag{17}$$

where the exponential function damps the eddy viscosity near the wall.

The channel height is H. The lengths of computational box in the streamwise and spanwise directions were chosen to be $L_x = \pi H$ and $L_z = 2\pi H/3$, respectively, based on two-point correlation measurements in laboratory experiments and the desire to capture all the important large eddies in the flow. The nondimensional grid spacings that result are $\Delta x^+ = 63$ and $\Delta z^+ = 42$, expressed in wall units. (The channel height H is 1280 wall units.) The grid spacing in the normal direction varies from $\Delta y^+ \approx 2$ near the wall to $\Delta y^+ \approx 50$ at the middle of the channel. The need for subgrid modeling is clear. Even near the wall, where grid is finely meshed in the normal direction, the horizontal spacing is not sufficient to resolve the experimentally observed wall streaks with a mean spanwise spacing of $\lambda_z^+ \approx 100$. Kim and Moin find, however, that wall streaks do appear in their simulation, but at a larger scale, the streaks apparently accommodating themselves to the available resolution.

The agreement of KM's simulation with laboratory measurements is remarkably good. After a time of evolution of $15.4H/U_c$ (U_c is the mean velocity of the center of the channel) KM obtain the mean-velocity profile (horizontally averaged) shown, along with experimental data, in Fig. 14. Near the wall the simulated profile is somewhat low; away from the wall a distinct logarithmic region is revealed with the correct slope (Kármán constant). The computed large-scale turbulent intensity profiles and the turbulent shear-stress profile are shown in Figs. 15 and 16, respectively. The $\langle \bar{u}''^2 \rangle^{1/2}$ and $\langle \bar{w}^2 \rangle^{1/2}$ profiles are in excellent agreement with experiment at all distances from the wall. (Superscript double prime denotes deviation from horizontal average.) In the wall region ($y^+ \lesssim 90$) the resolved vertical turbulence intensity is lower than experiment, possibly due to the fact that a significant amount of $\langle v^2 \rangle^{1/2}$ resides in the subgrid scales or that the subgrid model has deficiencies near the wall, as suggested by the deficit of the mean profile in this region.

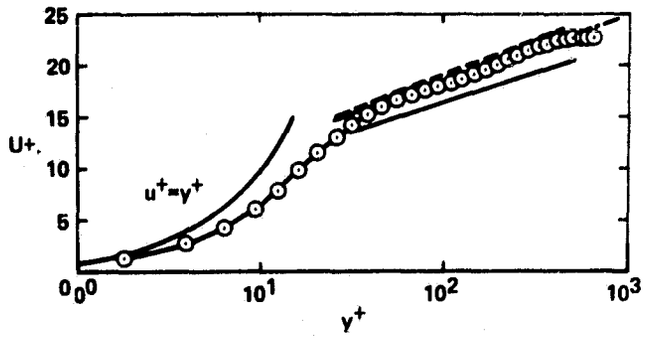

FIG. 14 Mean-velocity profiles; —⊙—, numerical simulation of [10]; experiment, ——, Re = 13800; — — —, Re = 57000; — — —, Re = 12200-61600.

Contour plots of instantaneous Reynolds stress $\bar{u}''\bar{v}$ reveal interesting phenomena. In a horizontal plane near the wall ($y^+ = 16$, Fig. 17) a number of hotspots occur where $\bar{u}''\bar{v}$ is large and negative. Kim and Moin determined that a great

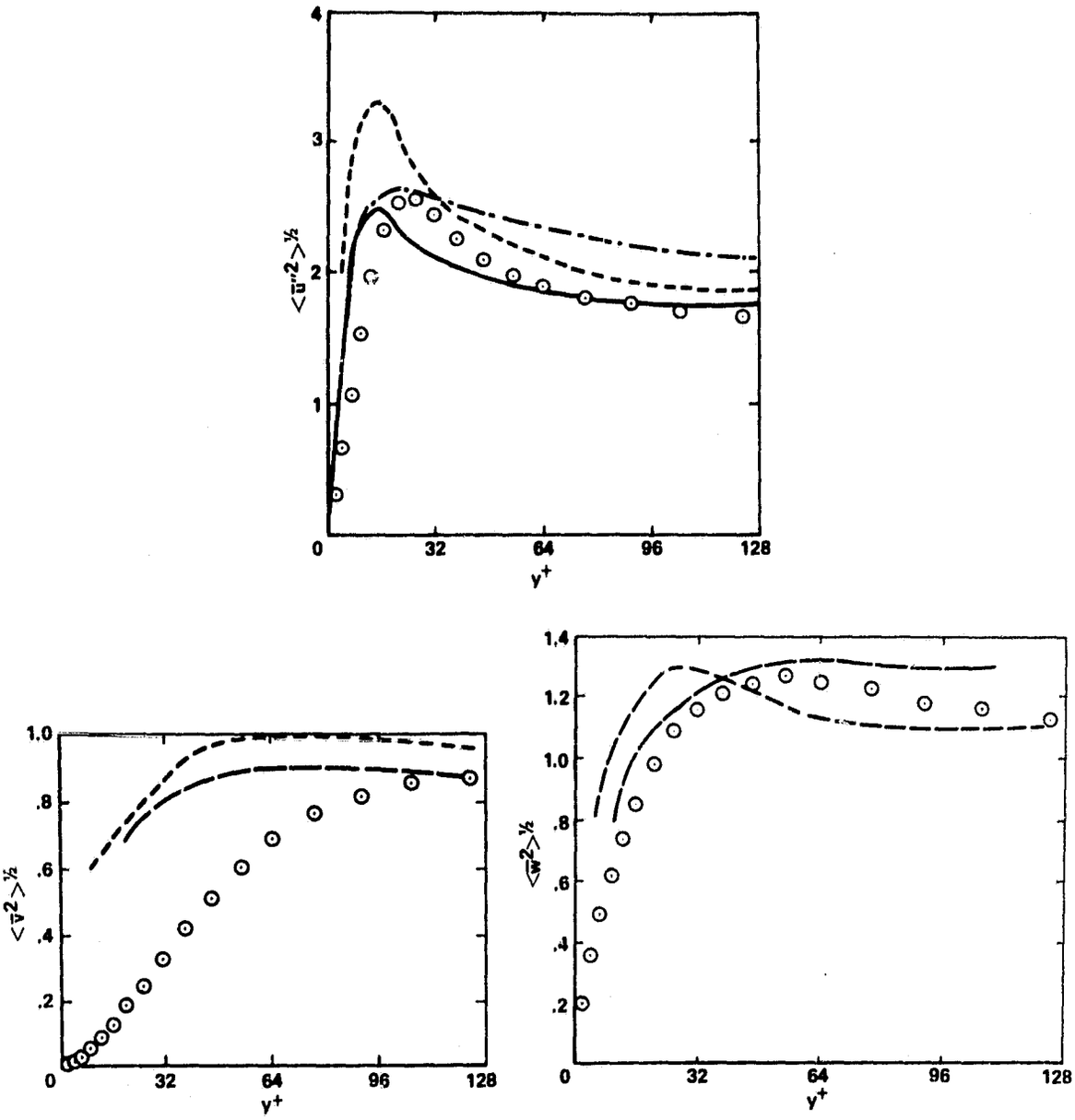

FIG. 15 Comparison of the horizontally averaged resolvable turbulence intensities normalized by u_τ with experimental data; ⊙, numerical simulation of [10]; experiment, ——, Re = 13800; — — —, Re = 15200; — — —, Re = 25000; — - —, Re = 120000.

majority of these active regions is associated with $\bar{u}'' > 0$, $\bar{v} < 0$, or "sweeps." Away from the wall ($y^+ = 90$, Fig. 18) the hotspots are associated with "bursts" or $\bar{u}'' < 0$, $\bar{v} > 0$. All these findings are in agreement with experiment [12].

Kim and Moin also investigated pressure-velocity gradient correlations in the region of $y^+ < 100$. These correlations provide for energy transfer between the individual components and turbulent energy and, as such, are of great interest to turbulence modelers. The computed correlations are shown in Fig. 19. Their behavior for $y^+ \gtrsim 20$ corresponds to the expected transfer from $\langle \bar{u}''^2 \rangle$ to $\langle \bar{v}^2 \rangle$ and $\langle \bar{w}^2 \rangle$. Close to the wall, however, KM show a substantial loss of $\langle \bar{v}^2 \rangle$ and a corresponding

gain of $\langle \tilde{w}^2 \rangle$ through the action of these correlations. By studying the fluid motion near the wall using "snapshots" or instantaneous contour plots, KM determined that the energy transfer was due to high-speed parcels of fluid approaching the wall and then spreading laterally ("splatting" effect).

D. Comparison of the Simulations

In Table I we compare a number of features of the three simulations. The natural length and time scales for the first two studies or the evolution of a disturbance in a

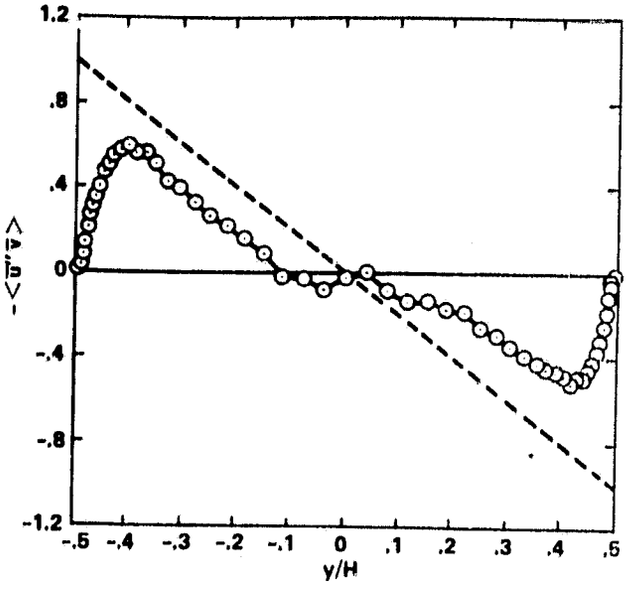

FIG. 16 Vertical profile of horizontally averaged resolvable turbulent shear stress.

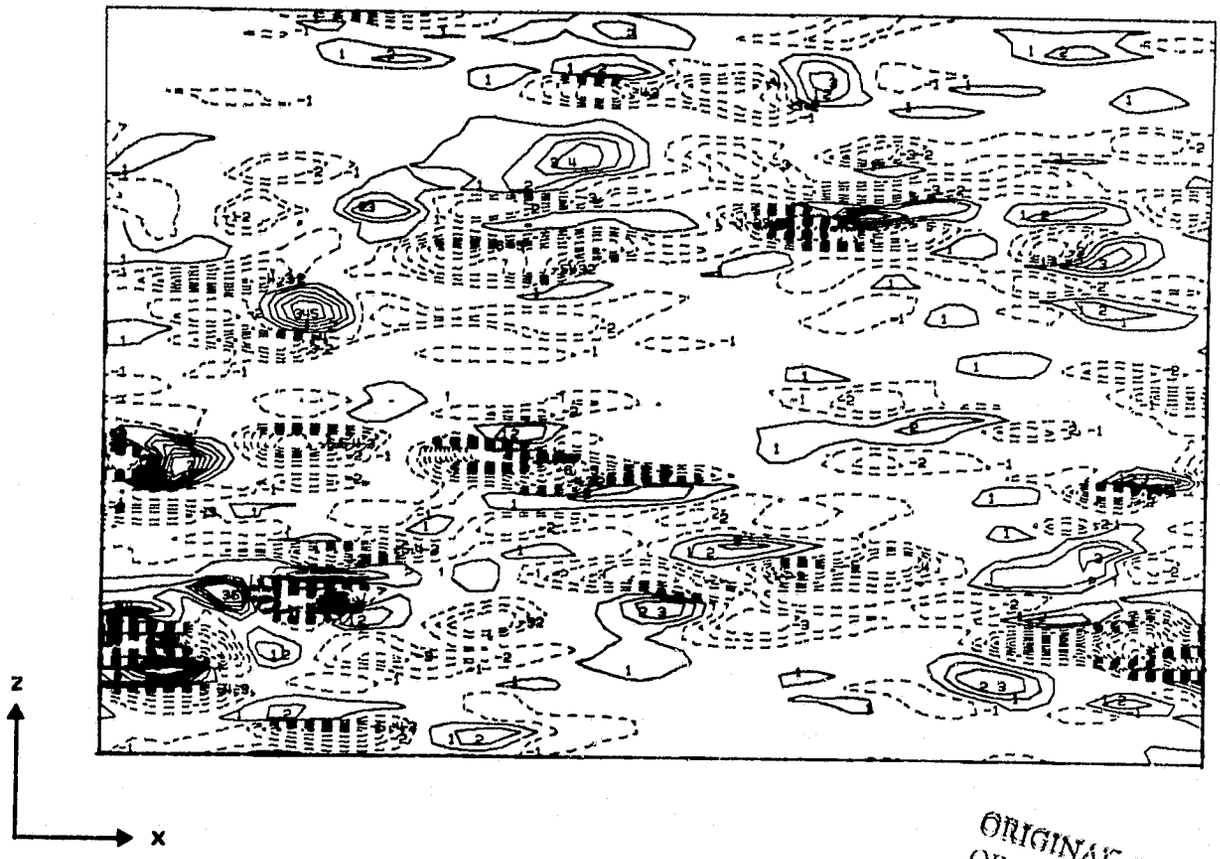

FIG. 17 Contours of $\tilde{u}''\tilde{v}$ in the x-z plane at $y^+ = 16$.

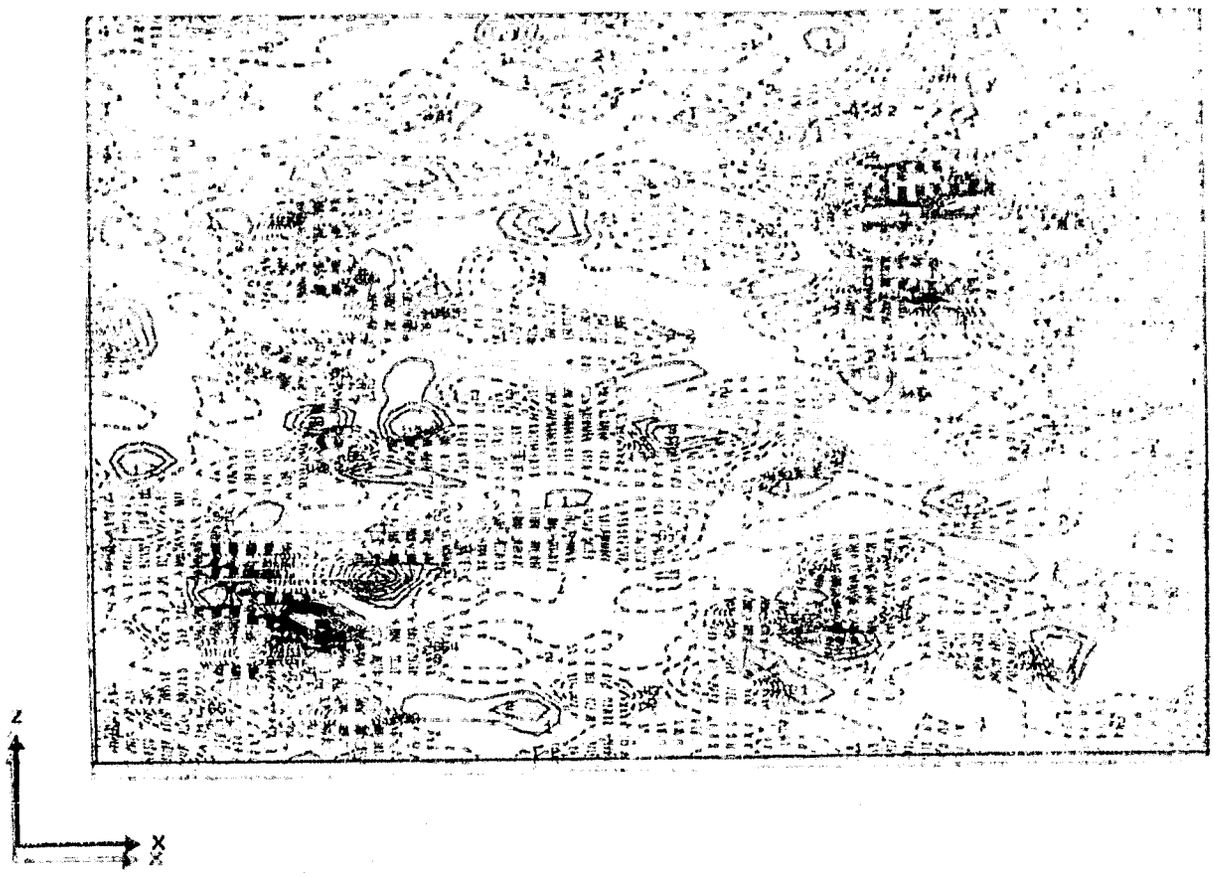

FIG. 18 Contours of $\bar{u}''\bar{v}$ in the x-z plane at $y^+ = 90$.

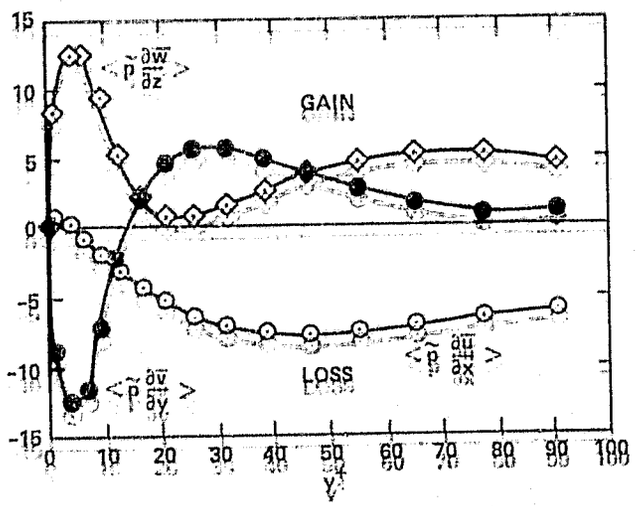

ORIGINAL PAGE IS
OF POOR QUALITY

FIG. 19 Vertical profiles of horizontally averaged, pressure-velocity gradient correlations in the vicinity of the wall ($y^+ \leq 100$).

TABLE I

SIMULATION PARAMETERS

	Wave disturbance	Spot disturbance	Channel flow
Grid			
$N_x \times N_y \times N_z$	64×128×64	500 filaments 8000 points (1/2 spot)	64×64×64
Mesh spacing			
$\Delta x/\delta^*$	0.39	0.41	---
$\Delta y/\delta^*$	$0.0078 \rightarrow \infty$	0.41	---
$\Delta z/\delta^*$	0.47	0.66	---
(wall units)			
Δx^+	16[a]	16[a]	63
Δy^+	$0.31 \rightarrow \infty$	16	$1.8 \rightarrow 50$
Δz^+	19	26	42
Turbulence volume (wall units^3)	0.3×10^9[b]	0.4×10^9[b]	12×10^9
Time step			
$\Delta t U_\infty/\delta^*$	0.24	0.49	---
Δt^+	0.38[a]	0.78[a]	0.61
Number steps/run	1500	100	2000
ILLIAC time/run, hr	12	2	12

[a] Estimate using $\delta^{*+} = (u_\tau/U_\infty)Re_{\delta^*} \approx 40$; $(\delta^*/U_\infty)^+ = (u_\tau^2/U_\infty^2)Re_{\delta^*} \approx 1.6$.

[b] Estimated vertical extent of turbulence = 250 wall units.

laminar boundary layer are δ^* and δ^*/U_∞, respectively. In the simulation of turbulent channel flow, appropriate length and time scales for the near-wall region are ν/u_τ and ν/u_τ^2, where u_τ is the wall friction velocity, $u_\tau = \sqrt{\nu\, \partial \langle u \rangle \partial y|_{wall}}$. To compare the transition studies with the channel flow simulation, the scales of the first two studies were converted to approximate turbulent scales as follows. Assume that the laminar boundary layer completes its transition to a turbulent layer. Then the original laminar displacement thickness in wall units is given by

$$\delta^{*+} = \frac{\delta^* u_\tau}{\nu} = \frac{u_\tau}{U_\infty}\frac{\delta^* U_\infty}{\nu}$$

$$= \frac{u_\tau}{U_\infty} \mathrm{Re}_{\delta^*}$$

$$\approx 40 \ ,$$

where we have used $u_\tau/U_\infty = 0.04$ for the turbulent layer and $\mathrm{Re}_{\delta^*} = 1000$. The time scale in wall units is found to be

$$\left(\frac{\delta^*}{U_\infty}\right)^+ = \frac{u_\tau^2}{U_\infty^2} \mathrm{Re}_{\delta^*}$$

$$= 1.6 \ .$$

Note that the two transitional studies have comparable resolution in the horizontal directions, but the vertical grid of WH is much finer. Both are able to resolve structures having length scales $O(\delta^*)$ in any direction, and, as shown in earlier figures, many such significant structures were found. Recall, for example, the vertical velocity contour plot (Fig. 5) at the two-spike stage of the study by WH, exhibiting large peak values ($\approx 0.21\ U_\infty$) and very large streamwise gradients. As shown in Fig. 20a, a similar structure with a peak v' of $0.42\ U_\infty$ was found in the spot simulation. The results are shown in a z-plane ($z = 0.8\ \delta^*$) containing mostly upward fluid motion (bursting ?) similar to the peak-plane behavior observed by WH. Contours of the perturbed spanwise vorticity are shown in Fig. 20b in the same x-y plane at $z = 0.8\ \delta^*$. As might be expected, the region of large $\partial v/\partial x$ is associated with a concentration of ω_z'.

The time evolution of the maximum vertical velocities is shown in Fig. 21. Also shown is the range of peak values in the

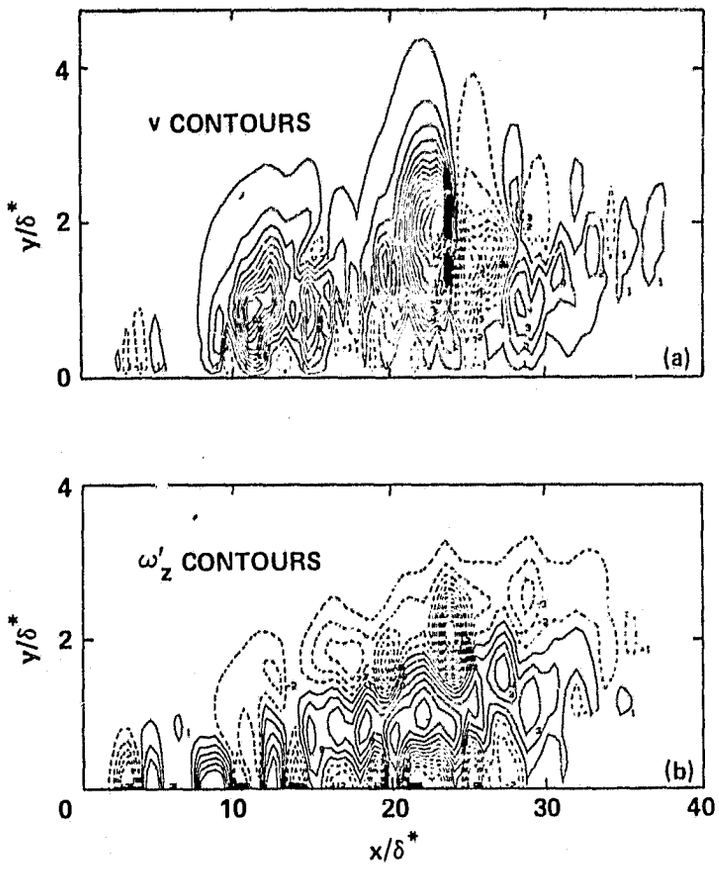

FIG. 20 Contours in an x-y plane from the numerical simulation of a spot-like disturbance: (a) vertical velocity; (b) perturbed spanwise vorticity.

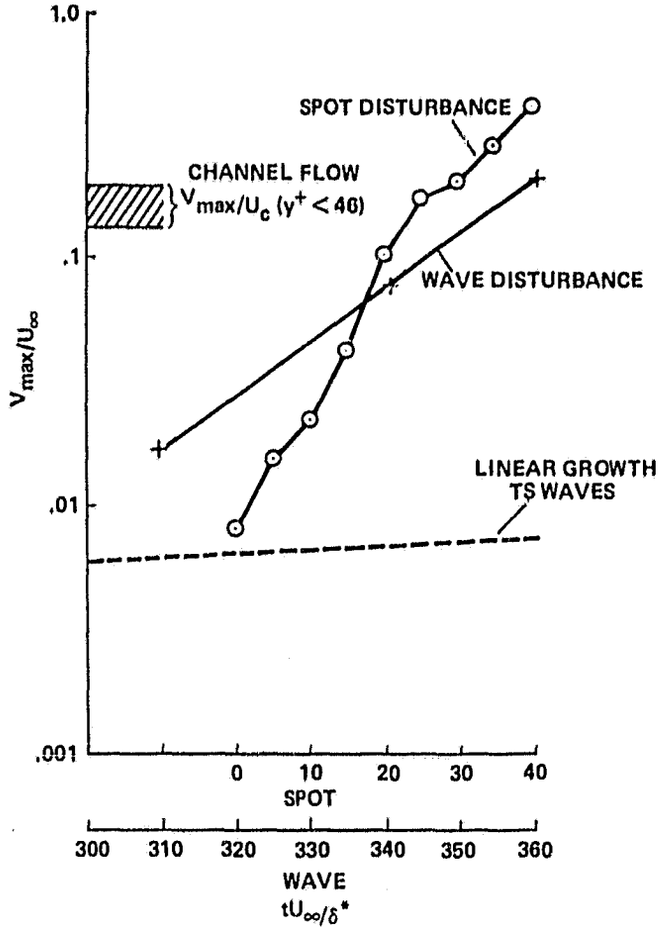

FIG. 21 Maximum vertical velocities in a plane.

channel flow simulation by KM in several y-z planes for $y^+ < 46$. Through the final stages of evolution the peak vertical velocity in the transition study of WH is experiencing exponential growth at 15 times the growth rate of the initial two-dimensional perturbation wave. Apparently this peak is associated with a small-scale ($O(\delta^*)$) secondary instability of the larger ($O(25\delta^*)$) slower-growing primary instability. The growth rate seen in the spot simulation is even larger and not exponential, presumably due to nonlinear interactions between small-scale perturbations.

Note that in the channel-flow study a relatively coarse mesh in the horizontal plane was used, clearly dictated by the relatively large volume of turbulence being simulated. A number of flow structures seen in the transitional studies that were ($O(\delta^*)$) and smaller in the spanwise and streamwise directions would not be resolved adequately by this mesh. (Recall that $\delta^{*+} \approx 40$.) Nevertheless, KM see in their simulation considerable turbulent activity near the wall, as evidenced by Figs. 15-19. As was mentioned above, turbulent structures do appear (wall streaks, etc.), but at a larger scale than in experiment, accommodating themselves to the available resolution. In Figs. 22 we see this effect illustrated in a contour plot of streamwise vorticity from KM's simulation. In Fig. 22a, about one seventh of the y-z computational plane is shown. Note that near the wall the spanwise extent of the cell-like structures is only a few times the smallest available scale in the span direction ($\Delta z^+ = 42$). In Fig. 22b a blowup of one of the more active regions near the wall is shown. With one exception, the structure is similar to the one shown in Fig. 9b from the spot simulation. The vertical scales in Figs. 22a and 22b have been expanded by a factor of 4 over the horizontal scales so that the actual structure depicted in Fig. 22b is considerably flattened. For comparison, Fig. 23 shows Fig. 9b from the spot simulation using the same scale in wall units of the channel-flow results. The smaller computational domain affords the luxury of seeing the fine-scale structures depicted in the figure.

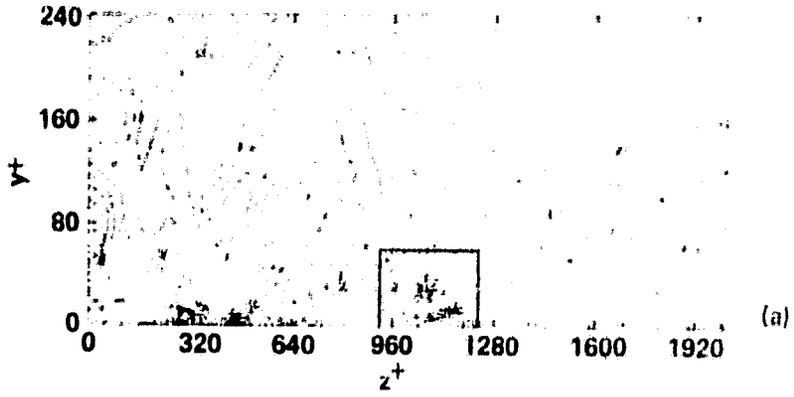

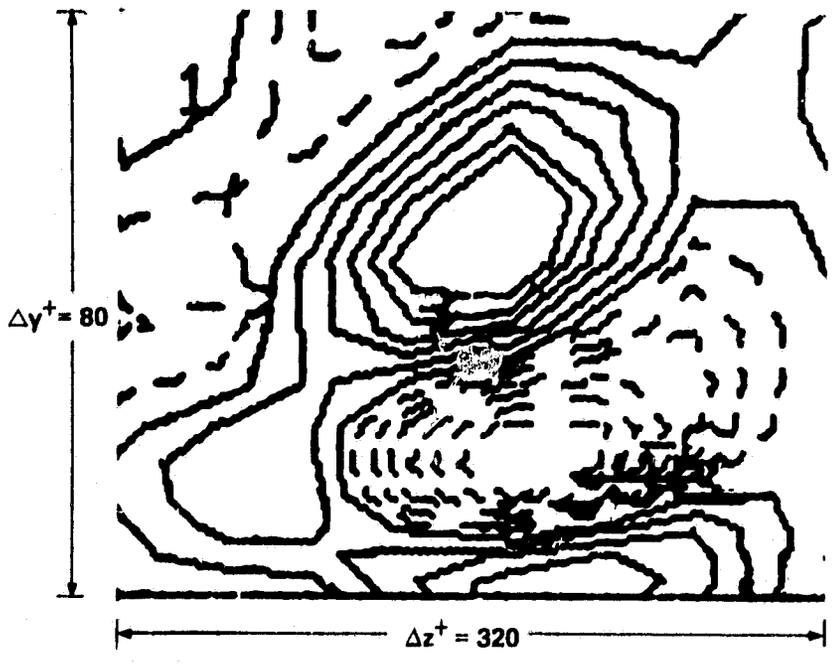

FIG. 22 Contours of streamwise vorticity in a y-z plane — channel-flow simulation of KM: (a) one seventh of computational plane; (b) blowup of region indicated.

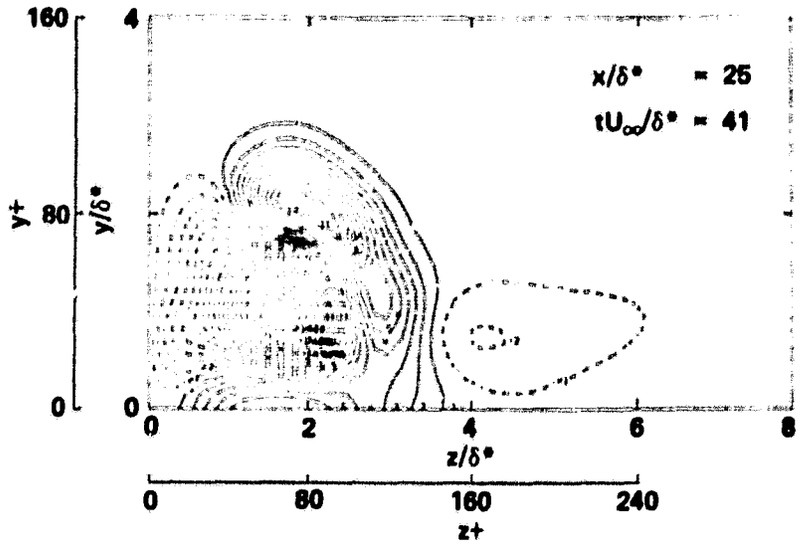

FIG. 23 Contours of streamwise vorticity in a y-z plane; spot simulation with scale in wall units.

III. EFFECTS OF SUBGRID-SUPERGRID SCALE MOTIONS

In the numerical simulation of fluid flows one can resolve only a limited range of length scales in the flow field. In most cases of interest, turbulent flows will contain important scales of motion outside this range. A major problem in the simulation of turbulent flows, therefore, is to model the effect of these subgrid or supergrid components on the resolvable scales. The objective of this modeling effort should be to minimize the error on any desired statistical information that is derived from the resolvable scale motions, including structural information. This problem appears particularly acute in the case of wall-bounded shear flows because of the importance of small-scale structures near the wall in the generation of turbulent energy and in turbulent mixing. In addition, the use of periodic boundary conditions will be a problem if scales larger than the computational domain are important.

In the first two studies discussed in the previous section, which were concerned with the transition of a laminar boundary layer, there was no explicit attempt to account for subgrid-scale effects. In the study by WH of the evolution of a wave-like disturbance, a Fourier representation was used for the dependence of the flow variables in the streamwise and spanwise directions. Thus, by the quadratic nonlinearity of the pressure and convective derivatives, the evolution of a given Fourier coefficient with two-dimensional wave number $\underline{k}_1$ within the resolved range ($k_{min} < |\underline{k}_1| \leq k_{max}$) will contain contributions from other wave numbers $\underline{k}_2$ and $\underline{k}_3$ satisfying

$$\underline{k}_2 + k_3 = \underline{k}_1 \ ,$$

if neither of the corresponding Fourier coefficients is negligible. If $\underline{k}_2$ and $\underline{k}_3$ are in the resolved range there is no problem. If either or both are out of the resolved range an error is made by neglecting this contribution. The assumption of streamwise periodicity leads to errors involving supergrid components. For the simulation of WH, this error (discussed in Section II) appears to be small. In flows where turbulent energy is simply cascading to higher wave numbers near the cutoff k_{max} (e.g., the decay of isotropic turbulence) the error involving subgrid components has the effect of turning off the cascade, resulting in a "pileup" of turbulent energy around $|\underline{k}| \gtrsim k_{max}$ in the numerical simulation. Several schemes, based on a Fourier representation of the flow variables, have been proposed to model the effects of the unresolved flow field ($|\underline{k}| > k_{max}$) and, therefore, to allow the turbulent cascade process to pass energy on to the subgrid scales. See Leslie and Quarini [13] for a discussion of these possibilities. In wall-bounded shear flows, however, the production of turbulent energy may also occur near the cutoff wave number. This poses an additional challenge to the capabilities of a subgrid model. In this case the model must account for all the important unresolved instability mechanisms that break up the wall shear layer and produce turbulence.

Again, in the vortex simulation of a spot-like disturbance no explicit model for the subgrid scales has been used as yet. Fine-scales of turbulence are produced automatically in the simulation as the space curves representing the vortex filaments take on highly convoluted configurations under the continual action of local velocity gradients. There is a lower limit to scale of turbulence that can be resolved, however. From Eq. (5) we see that this scale is the core radius of the filaments, σ. (Note that the Fourier transform of ω contains the factor $\exp(-|\underline{k}|^2\sigma^2/4)$ so the maximum resolved wave number is $\sim 1/\sigma$.) In the vortex simulation discussed in this paper some of the computed space curves representing vortex filaments had become highly stretched and contorted by the end of the simulation. More computational node points would be required to accurately follow the subsequent motion of these filaments. A less costly, alternative way of proceeding with the simulation would be to remesh the vorticity field, perhaps by smoothing the filament curves and by changing the topology of some curves [5]. Of course this procedure would be required repeatedly at later times as more fine scales reappear. The method appears to have promise as a subgrid modeling technique. Fine scales are allowed to develop in a natural way, retaining some interplay between the large and small scales. The method seems analogous to computing with a fine mesh in Eulerian calculation and periodically filtering out the high wave-number components of the velocity or vorticity field [14].

In the channel-flow simulation, KM use an eddy viscosity model for the subgrid-scale stresses. This model has proved adequate in less demanding situations, for example, the decay of homogeneous turbulence [15]. The model is successful in these cases in spite of the fact that it does a relatively poor job of estimating the actual point-wise subgrid-scale stresses computed by filtering the results of a fine-mesh simulation of a homogeneous turbulent flow [16,17]. Such a capability is, of course,

not a necessary requirement for a subgrid model, but it would be more encouraging if the correlation between the actual and modeled stresses was higher than the 30% level determined by McMillan and Ferziger [17]. A new model that does quite well in this respect has been proposed by Bardina et al. [18]. The idea is to model the subgrid stresses directly in terms of the small-scale component of the resolvable field.

In the simulation of KM, there is every indication the the eddy-viscosity model is quite satisfactory away from the wall ($y^+ \gtrsim 90$). The mean velocity and the three turbulence-intensity profiles agree well with experiment in that region. Near the wall, however, the mean velocity is low, as are the vertical velocity fluctuations. Apparently the eddy-viscosity model, being essentially dissipative, is not able to represent or account for important turbulent production processes near the wall that occur in the subgrid scales or in the smallest resolved scales where the interaction with the subgrid scales is of great importance. Evidence from the two studies concerning transition of a laminar boundary layer strongly suggests that that eventual breakup of the laminar layer involves structures that are $O(\delta^*)$ in the streamwise and spanwise directions. In KM's channel-flow simulation it is quite possible then that the lack of resolution in the x and z directions or other numerical effects or both inhibit the breakup of vorticity layers at the wall until they grow excessively thick. Indeed, in numerical experiments involving the filtering procedure, KM showed that substantial increases in turbulent shear stress near the wall are possible for short time intervals by modifying the treatment of the smallest resolved scales. It appears, therefore, that a subgrid model for the near-wall region should contain a destabilizing feature that would promote the breakup of vorticity layers rather than, or in addition to, the dissipative aspect of the eddy-viscosity model.

By using periodic boundary conditions in the horizontal directions, KM encountered errors due to unresolved supergrid components of turbulence. The magnitude of this error is not known, but is estimated to be small based on experimental two-point correlations.

IV. SUMMARY AND CONCLUSIONS

Numerical simulations of wall-bounded turbulent shear flows have confirmed the existence, and illuminated some of the characteristics, of cell-like substructures near the wall containing substantial vertical and streamwise vorticity. These structures appear to be responsible for or intimately related to many features of turbulent flows observed experimentally — intense vertical mixing, low-speed and high-speed streaks, and, hence, the streaky structures seen in photographs of dye-particle contaminants.

These structures were first revealed numerically in the simulation of turbulent channel flow. In this case, these structures seem to be related to strong ($-u'v$) hotspots and, ultimately, the mean-velocity profile since planar averages of $u'v$

yield the turbulent shear-stress profile. In the case of a turbulent spot, span-averaging over one cell produces a streamwise profile qualitatively similar to ensemble-averaged measurements of experiment.

In the simulation of the vibrating ribbon transitional flow all the features of the corresponding experiment were reproduced including the development of secondary instabilities with length scales $O(\delta^*)$. At this writing, Wray is investigating the properties of a strong streamwise vortical structure that he has located off the peak plane in the simulation of WH.

The impetus to simulate more complex wall-bounded shear flows in reasonable computer times means a continued sparseness of grid points for the near-wall region. More sophisticated subgrid-scale models will be required to account for the fine-scale structures discussed above that appear to be so important to the turbulent shear stress and turbulent mixing, in general, near the wall. Many interesting possibilities exist. We speculate that successful models will enhance the breakup of wall-bounded vorticity layers while perhaps retaining some aspects of an eddy-viscosity model.

ACKNOWLEDGMENT

The author thanks J. Kim, P. Moin, and A. Wray for many helpful discussions.

REFERENCES

1. A. WRAY AND M. Y. HUSSAINI, "Numerical Experiments in Boundary-Layer Stability," AIAA Paper 80-0275, AIAA 18th Aerospace Sciences Meeting, Pasadena, Calif., 1980.
2. S. A. ORSZAG AND L. C. KELLS, J. Fluid Mech. 96 (1980), 159.
3. L. S. G. KOVASZNAY, H. KOMODA, AND B. R. VASUDEVA, "Detailed Flow Field in Transition," Proceedings of the 1962 Heat Transfer and Fluid Mechanics Institute, 1962, pp. 1-26.
4. A. LEONARD, "Vortex Simulation of Three-Dimensional, Spotlike Disturbances in a Laminar Boundary Layer," in Turbulent Shear Flows II, L. J. S. Bradbury et al., eds., Springer-Verlag, Berlin, 1980, pp. 67-77.
5. A. LEONARD, J. Comput. Phys. (1980).
6. I. WYGNANSKI, M. SOKOLOV, AND D. FRIEDMAN, J. Fluid Mech. 78 (1976), 785.
7. B. CANTWELL, D. COLES, AND P. DIMOTAKIS, J. Fluid Mech. 87 (1978), 641.
8. S. J. KLINE, W. C. REYNOLDS, F. A. SCHRAUB, AND P. W. RUNSTADLER, J. Fluid Mech. 30 (1967), 741.
9. M. GAD-EL-HAK, R. F. BLACKWELDER, AND J. J. RILEY, "A Visual Study of the Growth and Entrainment of Turbulent Spots," Proceedings of IUTAM Symposium on Transition, Stuttgart, Germany, 1979.
10. J. KIM AND P. MOIN, "Large Eddy Simulation of Turbulent Channel Flow — ILLIAC IV Calculation," Proceedings of AGARD Symposium on Turbulent Boundary Layer — Experiment, Theory, and Modelling, The Hague, Netherlands, Sept. 24-27, 1979.
11. P. MOIN, W. C. REYNOLDS, AND J. H. FERZIGER, "Large Eddy Simulation of Incompressible Channel Flow," Report No. TF-12, Mechanical Engineering Department, Stanford U., Stanford, Calif., 1978.
12. R. S. BRODKEY, J. M. WALLACE, AND H. ECKELMANN, J. Fluid Mech. 63 (1974), 209.
13. D. C. LESLIE AND G. L. QUARINI, J. Fluid Mech. 91 (1979), 65.
14. B. FORNBERG, J. Comput. Phys. 25 (1977), 1.
15. N. N. MANSOUR, P. MOIN, W. C. REYNOLDS, AND J. H. FERZIGER, "Improved Methods for Large Eddy Simulations of Turbulence," in Turbulent Shear Flows I, F. Durst et al., eds., Springer-Verlag, Berlin, 1979, pp. 386-401.
16. R. A. CLARK, J. H. FERZIGER AND W. C. REYNOLDS, J. Fluid Mech. 91 (1979), 92.
17. O. J. McMILLAN AND J. H. FERZIGER, "Direct Testing of Subgrid Scale Models," AIAA Paper 79-072, New Orleans, La., 1979.
18. J. BARDINA, J. H. FERZIGER AND W. C. REYNOLDS, "Improved Subgrid-Scale Models for Large-Eddy Simulation," AIAA Paper 80-1357, Snowmass, Colo., 1980.

1. Report No.	2. Government Accession No.	3. Recipient's Catalog No.
NASA TM-81219		

4. Title and Subtitle	5. Report Date
TURBULENT STRUCTURES IN WALL-BOUNDED SHEAR FLOWS OBSERVED VIA THREE-DIMENSIONAL NUMERICAL SIMULATIONS	6. Performing Organization Code

7. Author(s)	8. Performing Organization Report No.
A. Leonard	A-8280

9. Performing Organization Name and Address	10. Work Unit No.
Ames Research Center, NASA Moffett Field, Calif. 94035	505-31-11-07
	11. Contract or Grant No.
	13. Type of Report and Period Covered
12. Sponsoring Agency Name and Address	Technical Memorandum
National Aeronautics and Space Administration Washington, D.C. 20546	14. Sponsoring Agency Code

15. Supplementary Notes

Presented at Turbulence Conference: The Role of Coherent Structures in Modeling of Turbulence and Mixing, Madrid, Spain, June 25-27, 1980.

16. Abstract

In the past few years, numerical techniques in fluid dynamics have matured to the point that meaningful simulations of three-dimensional transition or turbulent shear flows bounded by a wall are possible. At the same time, availability of advanced computers, over and above a CDC 7600-class machine, has allowed roughly a doubling of the spatial resolution in each direction, greatly enhancing the quality of the results.

We report on three recent simulations using the ILLIAC IV computer:

1. Study of boundary-layer stability and transition corresponding to vibrating-ribbon experiments.
2. Study of the evolution of a spot-like disturbance in a laminar boundary layer.
3. Investigation of turbulent channel flow.

A number of persistent flow structures have been observed in the above studies, including streamwise and vertical vorticity distributions near the wall, low-speed and high-speed streaks, and local regions of intense vertical velocity. The role of these structures in, for example, the growth or maintenance of turbulence is discussed. The problem of representing the large range of turbulent scales in a computer simulation is also discussed.

17. Key Words (Suggested by Author(s))	18. Distribution Statement
Boundary layer Turbulence, Transition Vorticity Numerical simulation	Unlimited STAR Category - 34

19. Security Classif. (of this report)	20. Security Classif. (of this page)	21. No. of Pages	22. Price*
Unclassified	Unclassified	29	$4.50

*For sale by the National Technical Information Service, Springfield, Virginia 22161